

Article

A Design Rule to Reduce the Human Body Effect on Wearable PIFA Antennas

Giovanni Andrea Casula *  and Giorgio Montisci

Dipartimento di Ingegneria Elettrica ed Elettronica, Università di Cagliari, Piazza D'Armi, 09123 Cagliari, Italy; giorgio.montisci@unica.it

* Correspondence: a.casula@diee.unica.it; Tel.: +39-070-675-5787

Received: 30 January 2019; Accepted: 14 February 2019; Published: 21 February 2019



Abstract: The robustness of wearable Ultra-High Frequency (UHF)-band planar inverted-F Antennas (PIFAs) with respect to coupling with the human body is an extremely difficult challenge for the designer. In this work a design strategy is presented to help the designer to adequately shape and extend the antenna ground plane, which has been derived by accurately analyzing the distribution of the electric and magnetic energy densities of the antenna in a region around the antenna borders. The optimal extension of the ground plane will be discussed for three different grounded antennas, both in terms of free space wavelength, and in terms of electric energy density magnitude. Following these rules, the antenna robustness with respect to the coupling with the human body can be significantly improved, but with a minimal impact on the antenna size. The antenna robustness has been successfully tested considering several models for the human phantom in the simulation environment. The numerical simulations, performed using Computer Simulation Technology (CST) Microwave Studio, have been confirmed by experimental data measured for one of the analyzed grounded antenna configurations.

Keywords: grounded antennas; PIFA antennas; wearable antennas; body-antenna coupling

1. Introduction

Recent advances in miniaturization of communicating devices and design of smart networks, allowed a rapid development of and a growing interest in body area networks and personal area networks, because of their very strong potential for several applications and services, such as personal healthcare, sport, space, entertainment, smart homes, and so on.

These applications require an easy integration into clothes of both antennas and sensors, as well as high-data-rate wireless devices, so that the wearer can be able to communicate wirelessly with several devices.

However, the proximity of the human body with the wearable antenna is a very difficult problem to face, as it can severely worsen the on-body device performance, and, consequently, the global performances of the system itself [1,2]. A wearable antenna should be designed to maximize its robustness with respect to the random variations in the body-antenna coupling scenario (due to the continuous changes in the distance between the antenna and the body caused by the wearer movements), because the radio link is greatly influenced by this coupling. In addition, each individual typically has different dielectric and geometrical parameters for the human body tissues [3,4].

The impact of the human body on the wearable antennas can be mitigated by enlarging the ground plane of the antenna, but this solution is not adequate in UHF applications, such as Radio Frequency Identification systems, because it could produce uncomfortable antennas for the wearer. Therefore, it would be extremely useful to the designer to have an effective design strategy, leading

to a suitable ground plane (and layout) configuration which guarantees simultaneously a satisfying robustness to the antenna-body distance variation, and a compact antenna size.

A design criterion to limit the effect of the coupling with the human body, is described in references [5–11], and consists of using an appropriate ground plane shape and size able to confine the electric energy density of the antenna in a region far from its border. These works, however, give no details about the design of the optimal antenna ground plane, which could allow the designer to obtain the best trade-off between compactness (i.e., wearability) and robustness with respect to the human body coupling. This is necessarily a compromise solution, because the antenna robustness increases for larger ground planes, but this improvement is in contrast with one of the most important requirements of wearable applications, i.e., the antenna size must be kept as small as possible.

The aim of this paper is to provide a reasonable compromise between the antenna robustness and its overall dimension. A preliminary work has been presented in reference [12], where numerical results on a PIFA antenna have been presented, comparing the antenna performance for different ground plane extensions, and relating this performance to the antenna energy density distribution.

The preliminary results presented in reference [12] are significantly extended and experimentally validated in this paper, and the optimal ground plane enlargement, required to design an antenna with an adequate robustness, will be discussed here for three different grounded antennas for wearable applications, both in terms of free space wavelength, and in terms of electric energy density amplitude. Finally, this paper also investigates if the choice of the human body phantom can affect the results, considering four different models for the human phantom, showing that the antenna robustness has a similar behavior for all the tested phantoms. Numerical simulations have been performed using CST Microwave Studio. While all the three PIFAs configurations considered here as the initial layouts of our numerical tests have been selected from the open scientific literature, where they have been already adequately tested and characterized both numerically and experimentally, one of the analyzed PIFAs has been experimentally characterized, obtaining a good agreement between numerical simulations and experimental validation. This confirms the usefulness of the proposed design strategy.

2. Numerical Simulation Results

In this section, the energy-based design criteria derived in reference [7] for wearable UHF-Band PIFAs, which provide a general strategy to increase the antenna robustness regardless of the optimization of the antenna dimension, have been extended to find an optimal dimension and shape for the antenna ground plane, which allows us to achieve the best trade-off between the antenna size and its robustness.

The idea proposed here to increase the antenna robustness, obtaining at the same time an optimal dimension and shape for the antenna ground plane, consists of extending the antenna layout following the “profile” of the electric energy density in the antenna near-field region close to the ground plane border. The first step of this optimization process is an adequate enlargement of the ground plane, which must be extended enough to include almost all the electric energy density around the antenna borders. After this ground plane extension, the distribution of the energy density over the enlarged ground plane is analyzed, and a suitable threshold is defined for the amplitude of the electric energy density, in correspondence of which the ground plane is truncated. It will be shown that a further extension of the ground plane is not required, since the resulting increase in the antenna robustness is negligible enough for ground plane extensions, which include values of the electric energy density beyond the selected threshold. Therefore, this strategy allows us to obtain a good compromise solution between antenna robustness and size and can be considered a general rule connecting the energy density amplitude with the optimal ground plane extension.

The proposed design rule has been successfully applied in this paper to three PIFAs from the open literature. The PIFAs under test span a wide fraction of the UHF spectrum for wearable antenna applications and are, specifically, two RFID tag antennas operating in the UHF band [7,13,14], and a folded PIFA for on-body communications working at 2.4 GHz [7,15].

To account for the presence of the human body, the simplified three-layer model already used in [7] has been considered in the simulated environment, as shown in Figure 1. It is composed of

- skin layer ($\epsilon_r = 41.32$, $\sigma = 0.855$ S/m @ 900 MHz) with a thickness of 1.5 mm
- fat layer ($\epsilon_r = 5.46$, $\sigma = 0.05$ S/m @ 900 MHz) with a thickness of 20 mm
- muscle layer ($\epsilon_r = 54.97$, $\sigma = 0.934$ S/m @ 900 MHz) with a thickness of 30 mm

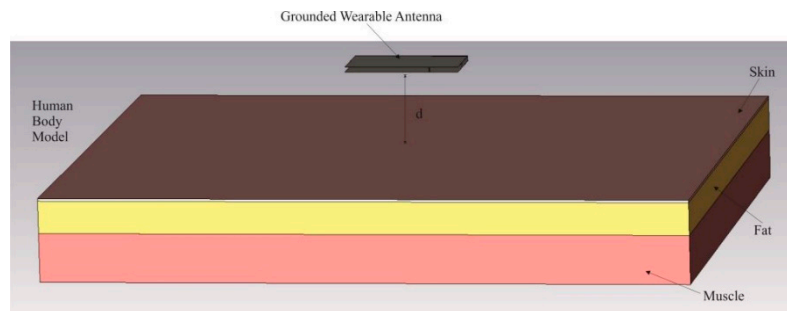


Figure 1. A wearable antenna on the phantom model used to perform the numerical investigation of the antenna robustness to the body proximity.

The robustness of each antenna with respect to the human body proximity has been evaluated by computing two key parameters for different antenna distances, d , from the phantom, as indicated in Figure 1. These parameters are the radiation efficiency, and the power transmission coefficient, τ , defined as:

$$\tau = 1 - \left| \frac{Z_{IN} - Z_0}{Z_{IN} + Z_0} \right|^2 \quad (1)$$

where in Z_{IN} is the antenna input impedance, and Z_0 is a reference impedance, equal to the antenna input impedance at the resonance frequency ($Im(Z_{IN}) = 0$) when the antenna is adherent to the human body model ($d = 0$ mm).

The best ground plane configuration is the one exhibiting a reasonable value of $\tau \times \eta$, with a τ as great as possible, with both stable (or increasing) with respect to the antenna-body distance, d .

2.1. Wearable Planar Inverted-F Antenna at UHF Frequencies

The first antenna under test is a PIFA antenna suitable for wearable tags at UHF frequencies [13]. The geometrical parameters used in the numerical simulations are summarized in Figure 2, and the electric and magnetic energy densities are shown in Figure 2c,d, respectively. The electric energy density shows a single peak, close to the antenna open end, whereas the magnetic energy density shows two peaks, each one close to the antenna lateral edges.

In order to choose the optimal profile for the ground plane extension, the ground plane must be enlarged enough to include the great part of the electric energy density around the antenna borders. In Figure 3a, the electric energy density is reported when the ground plane extension is equal to $\Delta L = 40$ mm. This extension allows us to take into account the most of the electric energy density distribution around the antenna borders, which is the magnitude of the energy in the borders lower than 10^4 times the electric energy density peak, as shown in Figure 3a,b, where the energy distribution is plotted with different scales. The maximum of the electric energy density is in fact 1.5×10^{-4} J/m³ (Figure 3a), while the value of the energy density at the upper border of the elongated ground plane is lower than 1.0×10^{-7} J/m³ (Figure 3b). Considering this energy distribution, a suitable threshold must be defined for the amplitude of the electric energy density, and the ground plane is truncated in correspondence with the values of the electric energy density equal to this threshold, as indicated in Figure 3c, where the normalized electric energy density on the ground plane for the antenna with $\Delta L = 40$ mm is represented with contour lines. A reasonable choice for this threshold is a value which is a thousand times lower than the absolute maximum of the electric energy density (i.e., 1.5×10^{-7} J/m³,

as indicated in Figure 3b), because the ground plane areas on which the values of energy density are lower than this threshold and can be reasonably neglected.

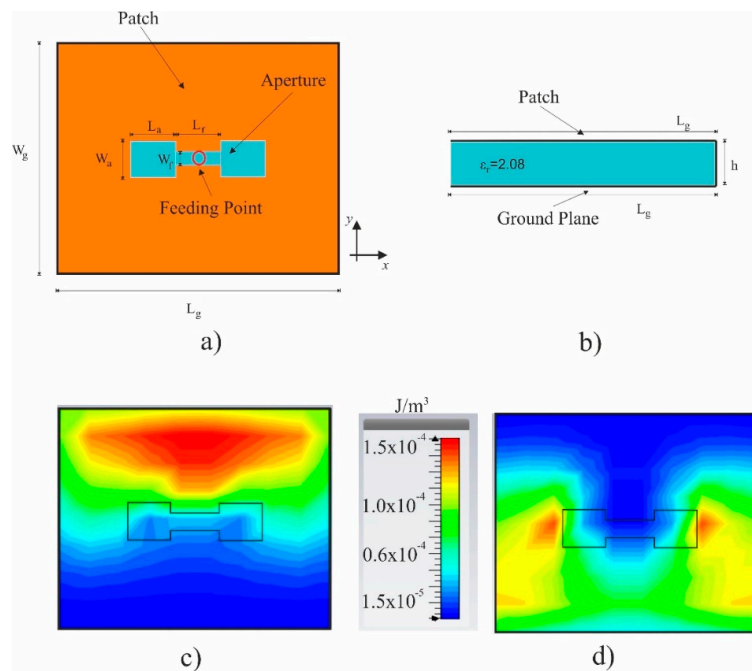


Figure 2. Front view (a), and lateral view (b) of the considered antenna. (c) Electric and (d) Magnetic energy densities close to the ground plane, at the resonant frequency. $W_g = 49$ mm, $L_g = 60$ mm, $W_a = 8$ mm, $L_a = 10$ mm, $W_f = 3$ mm, $L_f = 10$ mm, $h = 4$ mm.

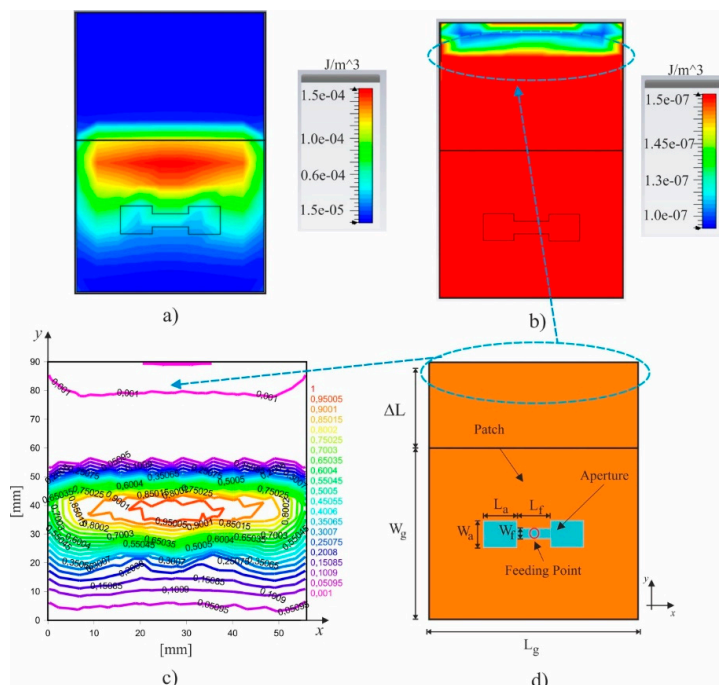


Figure 3. (a) Electric energy density on the ground plane for the antenna with $\Delta L = 40$ mm. (b) Electric energy density on the ground plane for the antenna with $\Delta L = 40$ mm with the maximum peak set to a value 10^3 times lower than the one shown in (a). (c) Normalized Electric energy density on the ground plane for the antenna with $\Delta L = 40$ mm represented with contour lines. (d) Profile of the extended ground plane following the electric energy density shown in (b), with $\Delta L = 30$ mm.

For wearable applications, the antenna size is a very strict requirement, and the wearable antenna should be as comfortable and unobtrusive as possible for the wearer. For this reason, it is very important to evaluate the optimal ground plane extension. It is also necessary to design an antenna with an adequate robustness, not only in terms of free space wavelength, but also in terms of electric energy density magnitude. Moreover, this choice is also frequency independent. For the considered antenna, the ground plane extension which follows the profile of the electric energy density, obtained using a threshold a thousand times lower than the absolute maximum of this energy density, is equal to $\lambda/10$ at the center frequency (30 mm at 963.5 MHz), as indicated in Figure 3. It will be shown that this enlargement of $\lambda/10$ is adequate to ensure a very good robustness for all the tested antennas, and, therefore, it can be used as a “rule-of-thumb” in the design of robust grounded wearable antennas.

To evaluate the increase on antenna robustness due to different ground plane extensions, in Figures 4–6 a parametric analysis of the PIFA antenna shown in Figure 2 has been performed, by varying the extension ΔL of the structure towards the vertical direction (which is the direction of the maxima of the electric energy density), as shown in Figure 3. The variations of τ (Figure 4), η (Figure 5), and $\tau \times \eta$ (Figure 6) with respect to the distance d from the human body are shown, and it is apparent that the robustness of the antenna with respect to the presence of the human body can be significantly increased if the ground plane is extended towards the antenna section corresponding to the location of the maximum of the electric energy density. As expected, the antenna robustness increases along with increasing values of the ground plane enlargement. However, the results obtained using a large ground plane extension ($\Delta L = 40$ mm), and the extension which follows the profile of the electric energy density ($\Delta L = 30$ mm) are comparable in terms of antenna robustness. Therefore, the enlargement of the ground plane which follows the profile of the electric energy density, equal to $\Delta L = 30$ mm = $\lambda/10$ (λ being the free space wavelength at 963.5 MHz), can be reasonably considered an optimal ground plane extension, giving a very good compromise between the antenna robustness and its overall dimension. On the other hand, when the size of the antenna is a critical issue, the results shown in Figures 4–6 suggest that even smaller extensions can be used, still preserving an adequate robustness of the structure. As an example, also with a minimal extension of $\Delta L = \lambda/20$ (corresponding to only 15 mm at 963.5 MHz), the obtained antenna presents a discrete input matching (τ decreases to 0.65 for $d = 50$ mm), and the efficiency parameter $\tau \times \eta$ keeps close to 0.3. This behavior can be still considered to be satisfactory, especially if compared with the PIFA antenna without any extension, whose performance is extremely degraded by the human body proximity, both in terms of input matching and radiation efficiency (τ becomes lower than 0.6 for d only equal to 5 mm, while $\tau \times \eta$ is around 0.1).

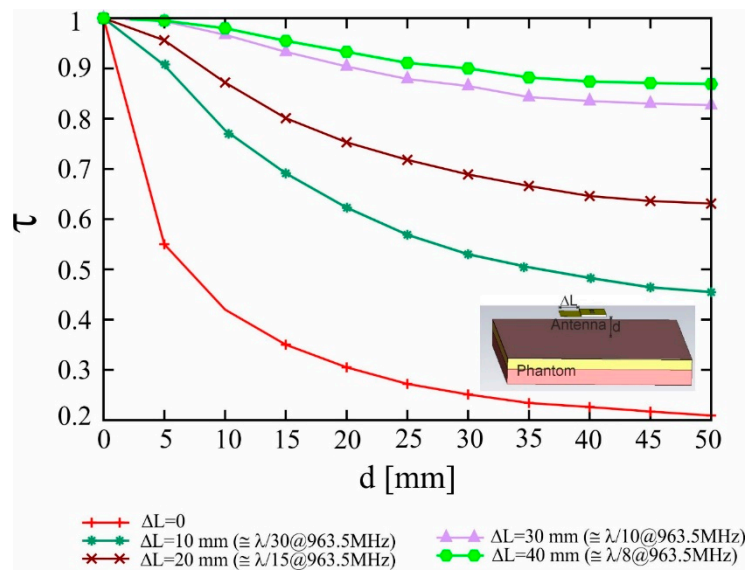


Figure 4. τ with respect to the distance from the body phantom for different extensions of the antenna ground plane.

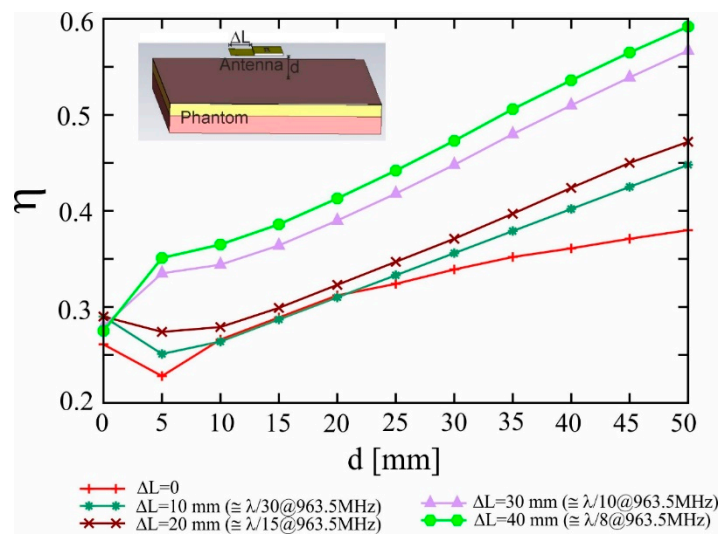


Figure 5. η with respect to the distance from the body phantom for different extensions of the antenna ground plane.

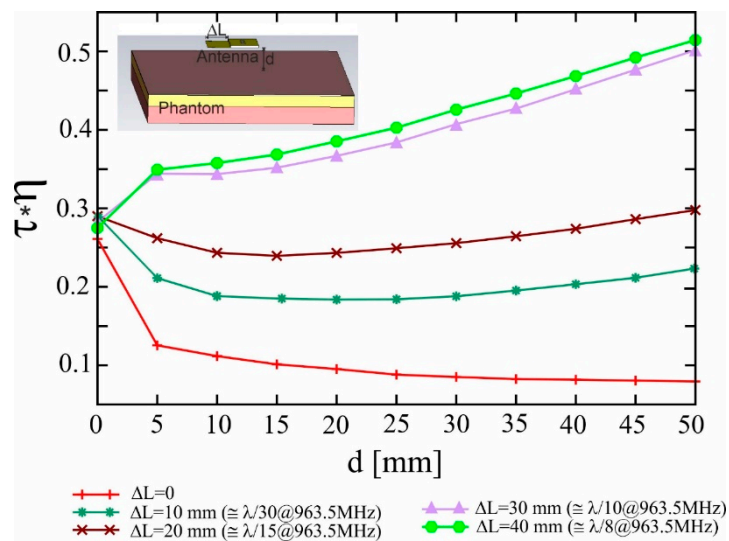


Figure 6. $\tau \times \eta$ with respect to the distance from the body phantom for different extensions of the antenna ground plane.

2.2. Standard Planar Inverted-F Antenna at UHF Frequencies

The above analysis has been repeated for a PIFA-type tag antenna working in the UHF frequency band [14]. The original configuration proposed in reference [14] (and reported in Figure 7) has been modified by reducing the ground plane size to exactly fit the radiating patch dimension ($W_g = W_p$ and $L_g = L_p$). The electric and magnetic energy densities are shown in Figure 7d,e, respectively. As expected for a standard PIFA, the maximum of the electric energy density is close to the antenna open end, whereas the maximum of the magnetic energy density is close to the antenna shorting edge. Also in this case, the optimal profile for extending the ground plane has been chosen after analyzing the electric energy density distribution of the antenna with a ground plane enlargement equal to $\Delta L = 40$ mm (Figure 8a), since this extension allows to take into account the great part of the electric energy density around the antenna borders. The same threshold of Section 2.1 has been chosen (i.e., a value which is thousand times lower than the absolute maximum of the electric energy density), and the ground plane has been cut in correspondence of the values of the electric energy density equal to this threshold (Figure 8c). This threshold corresponds to an extension equal to $\lambda/10$ at the center frequency of 916.25 MHz (32.5 mm), as in the case of Section 2.1.

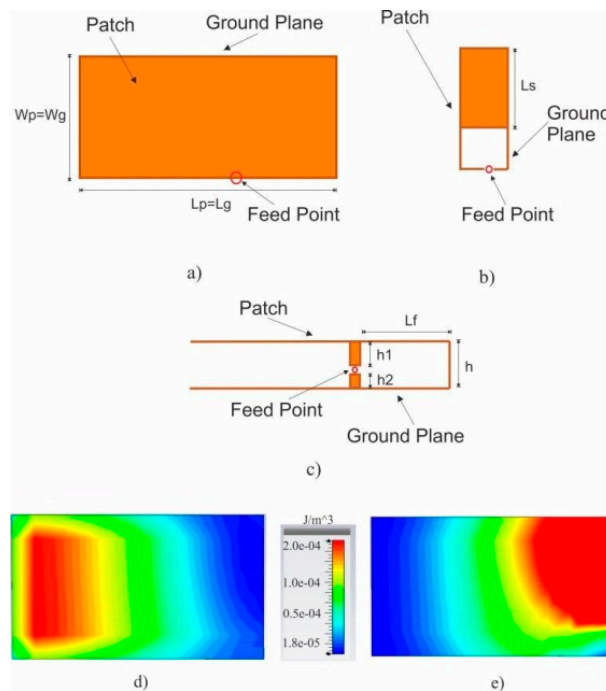


Figure 7. Top view (a), and side view (b), (c) of the considered antenna. Electric (d) and Magnetic (e) energy densities on the antenna ground plane, at the resonant frequency. $W_p = W_g = 40$ mm, $L_p = L_g = 70.5$ mm, $L_s = 24$ mm, $L_f = 17.5$ mm, $h_1 = 2.465$ mm, $h_2 = 0.1$ mm, $h = 3$ mm.

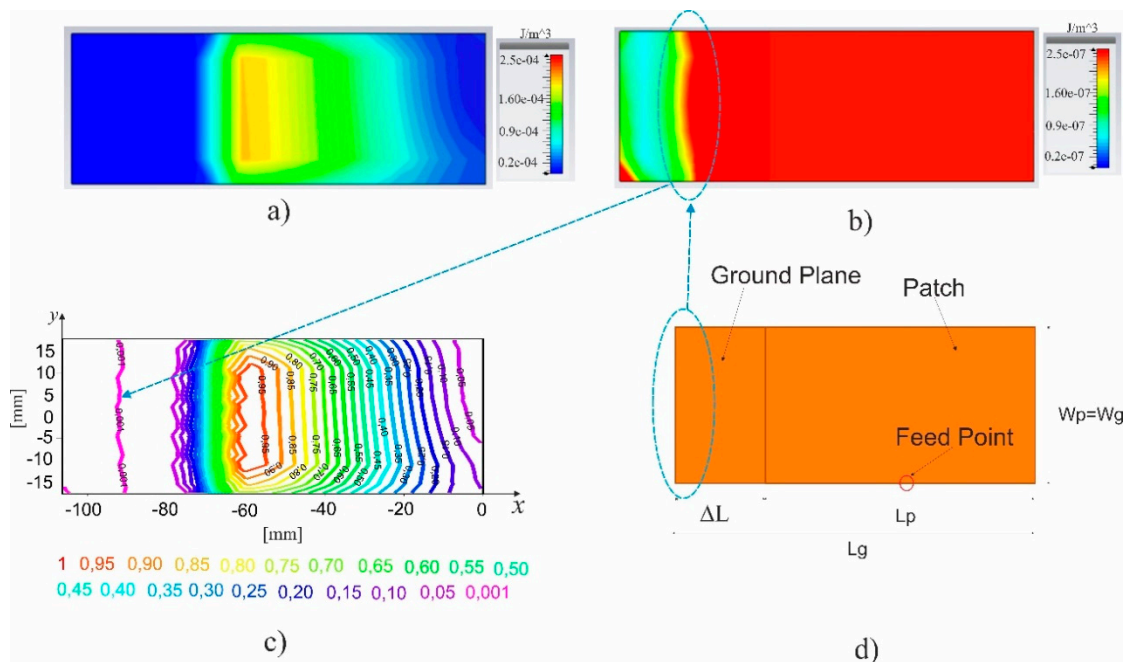


Figure 8. (a) Electric energy density on the ground plane for the antenna with $\Delta L = 40$ mm. (b) Electric energy density on the ground plane for the antenna with $\Delta L = 40$ mm with the maximum peak set to a value 10^3 times lower than the one shown in (a). (c) Normalized electric energy density on the ground plane for the antenna with $\Delta L = 40$ mm represented with contour lines. (d) Profile of the extended ground plane following the electric energy density shown in (b), with $\Delta L = 32.5$ mm.

In order to study the effect of the enlargement of the ground plane on the antenna robustness, in Figures 9–11 a parametric analysis of the PIFA antenna shown in Figure 7 has been performed, by varying the extension ΔL of the structure towards the horizontal direction (which is the direction

of the maxima of the electric energy density), as shown in Figure 8. The variations of τ (Figure 9), η (Figure 10), and $\tau \times \eta$ (Figure 11) with respect to the distance d from the human body are shown. Also in this case, the results obtained for $\Delta L = 40$ mm (large ground plane extension) and for the extension which follows the profile of the electric energy density ($\Delta L = 32.5$ mm) are very similar, and even a minimal extension of $\lambda/20$ (corresponding to only 16 mm at 916.25 MHz), can ensure a significant improvement of the antenna robustness if compared with the PIFA antenna without any extension (see Figures 9–11).

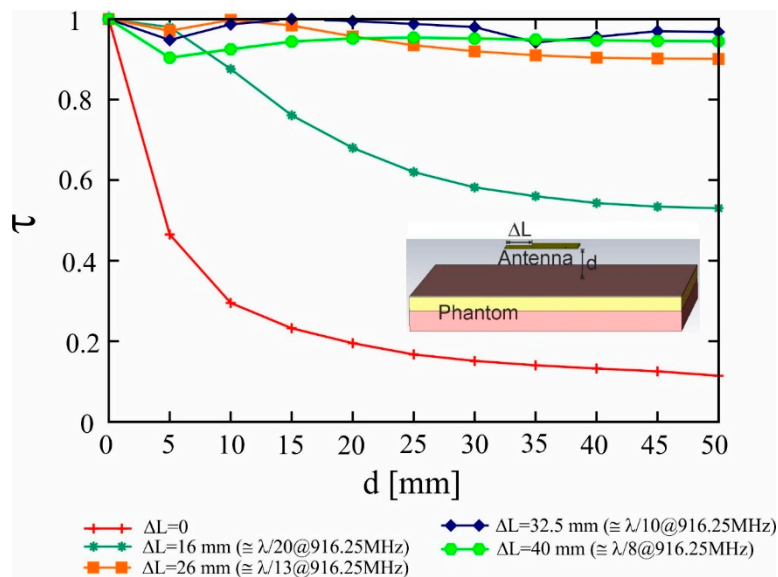


Figure 9. τ with respect to the distance from the body phantom for different extensions of the antenna ground plane.

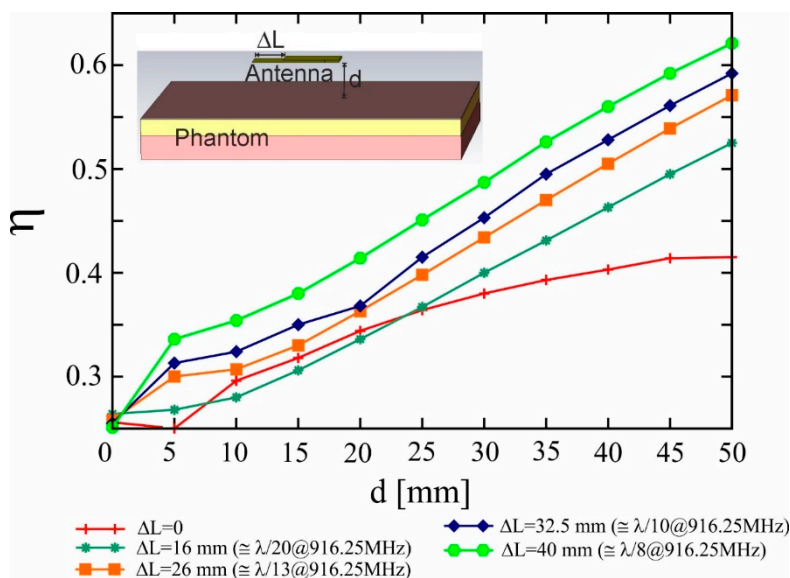


Figure 10. η with respect to the distance from the body phantom for different extensions of the antenna ground plane.

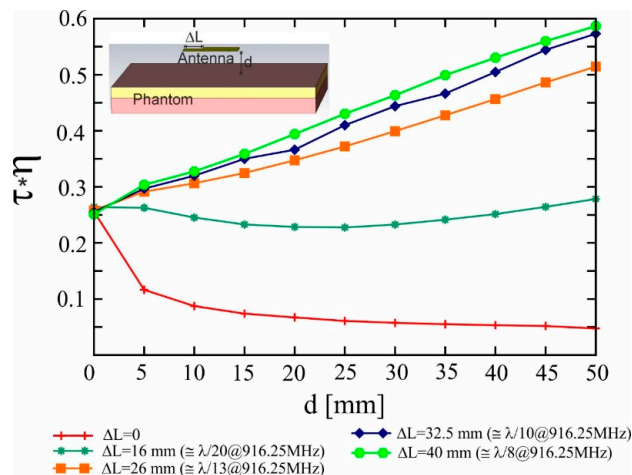


Figure 11. $\tau \times \eta$ with respect to the distance from the body phantom for different extensions of the antenna ground plane.

2.3. Planar Inverted-F Antenna at 2.45 GHz

The analysis of Sections 2.1 and 2.2 has been performed also to a folded PIFA for on-body communications at 2.45 GHz [15]. The geometrical parameters used in the numerical simulations, the antenna layout, and the electric and magnetic energy densities are shown in Figure 12. The magnetic energy density shows a single peak close to the antenna shorting edge, whereas the electric energy density shows two peaks, with each one close to the antenna lateral edges. The optimal profile for the ground plane extension has been chosen after analyzing the electric energy density for the antenna with $\Delta L = 20$ mm (Figure 13a,b), since this extension allows us to take into account the major part of the electric energy density around the antenna borders. The same threshold of Sections 2.1 and 2.2 has been chosen (i.e., a value which is 10^3 times lower than the absolute maximum of the electric energy density), and the ground plane has been cut in correspondence of the values of the electric energy density equal to this threshold (Figure 13c). Again, this threshold corresponds to an extension equal to $\lambda/10$ at the center frequency (12.5 mm at 2.45 GHz).

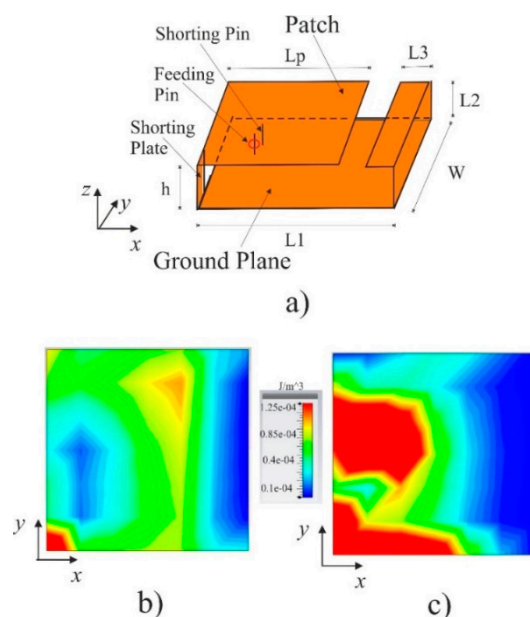


Figure 12. 3D view (a), of the considered antenna. (b) Electric and (c) Magnetic energy densities close to the ground plane, at the resonant frequency. $L_1 = 26$ mm, $L_2 = 3.5$ mm, $L_3 = 2.5$ mm, $W = 26$ mm, $L_p = 20.5$ mm, $h = 3.5$ mm.

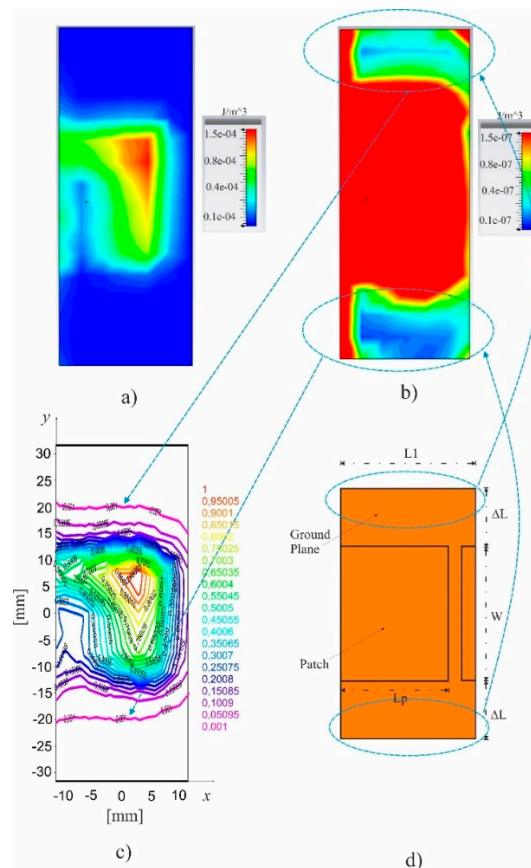


Figure 13. (a) Electric energy density on the ground plane for the antenna with $\Delta L = 20$ mm. (b) Electric energy density on the ground plane for the antenna with $\Delta L = 20$ mm with the maximum peak set to a value 10^3 times lower than the one shown in (a). (c) Normalized electric energy density on the ground plane for the antenna with $\Delta L = 20$ mm represented with contour lines. (d) Profile of the extended ground plane following the electric energy density shown in (b), with $\Delta L = 12.5$ mm.

In Figures 14–16 a parametric analysis of the PIFA antenna shown in Figure 12 has been performed, by varying the extension ΔL of the structure towards the vertical direction (which is the direction of the maxima of the electric energy density), as shown in Figure 13. The variations of τ (Figure 14), η (Figure 15), and $\tau \times \eta$ (Figure 16) with respect to the distance d from the human body are shown, and confirm that, also for this third presented example, the robustness of the antenna increases for increasing values of the ground plane enlargement, but the performance between the configuration with a large ground plane extension ($\Delta L = 20$ mm), and the configuration with an extension which follows the profile of the electric energy density ($\Delta L = 12.5$ mm) is very similar. Also in this case, even a minimal extension (for example $\lambda/30$, corresponding to only 4 mm at 2.45 GHz), can ensure a good improvement of the antenna robustness if compared with the PIFA antenna without any extension. Despite this, the folded PIFA (due to its folded layout) also presents a discrete robustness without any ground plane enlargement.

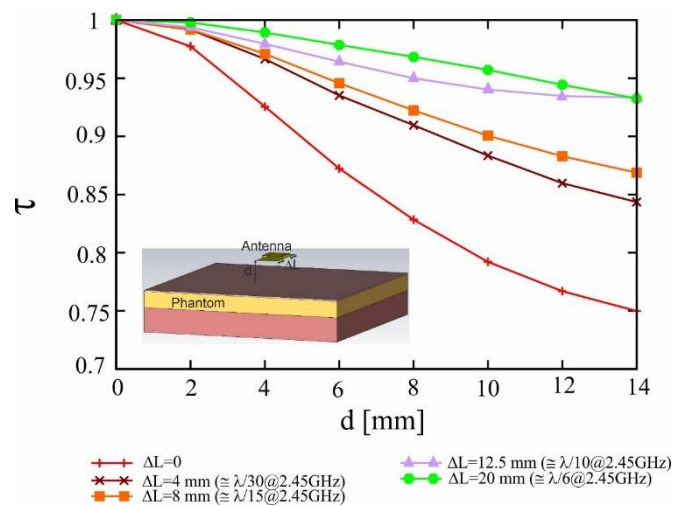


Figure 14. τ with respect to the distance from the body phantom for different extensions of the antenna ground plane.

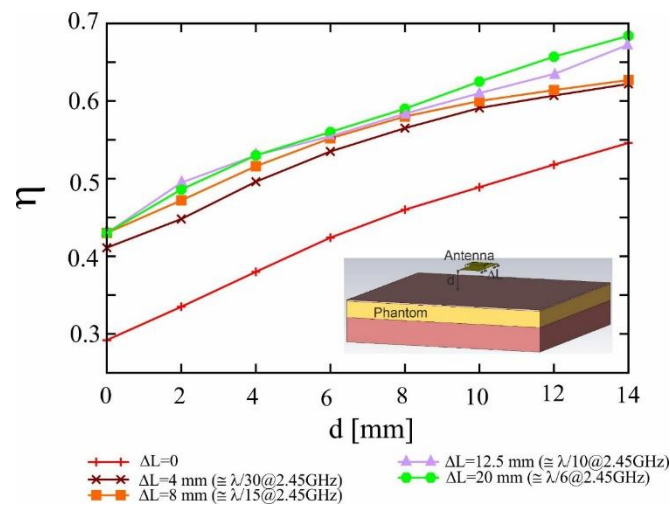


Figure 15. η with respect to the distance from the body phantom for different extensions of the antenna ground plane.

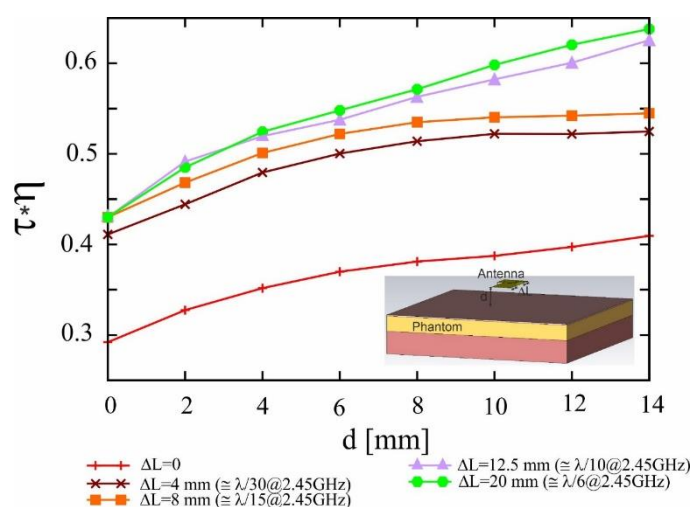


Figure 16. $\tau \times \eta$ with respect to the distance from the body phantom for different extensions of the antenna ground plane.

Three different examples, with different antenna layouts and different operating frequencies, have been investigated to find a criterion for increasing the antenna robustness with respect to the human body proximity, obtaining at the same time an optimal dimension and shape for the antenna ground plane. The choice of the proper shape and extension of the antenna ground plane have been derived by accurately analyzing the distribution of the electric and magnetic energy densities of the antenna in a region around the antenna borders. The best compromise solution is to extend the ground plane following the profile of the electric energy density, since with this choice it is possible to obtain a very robust antenna while also reducing its overall size. The optimal extension of the ground plane has been evaluated both in terms of free space wavelength, and in terms of electric energy density magnitude, and for the three discussed examples the same values have been obtained, namely:

- an optimal enlargement equal to $\lambda/10$;
- an optimal threshold equal to 10^{-3} times of the maximum value of the electric energy density.

It is worth highlighting that the previous design rules are frequency independent, and therefore can be very helpful for the designer, because they can be applied to general antenna layouts, and for different applications in a wide range of operating frequencies. Following these rules, the antenna robustness with respect to the coupling with the human body can be significantly improved, but with a minimal impact on the antenna size.

3. Experimental Validation

The PIFAs considered in Section 2.1, Section 2.2, and Section 2.3 as the initial layouts of our numerical tests have been already completely characterized, both numerically and experimentally, since they have been selected from the open scientific literature. The PIFA antenna analysed in Section 2.1 will be experimentally characterized.

Therefore, a prototype of the antenna in Figure 3d has been realized (Figure 17a), and the commercial chip “Impinji Monza 4” has been soldered to the antenna gap. We used the same measurement setup of [10], where the human tissue has been experimentally simulated by using a simplified phantom, consisting of a PVC tank of dimension 25 cm \times 15 cm \times 10 cm, having a thickness of 1 mm, filled up with a tissue-simulating liquid with muscle-like parameters at 870 MHz ($\epsilon_r = 56.6$, $\sigma = 1.33$ S/m), made with deionized water (53%), saccharose (45.6%) and sodium chloride (1.4%) [16]. This solution allows us to place the liquid phantom as close as possible to the antenna, and the minimum achievable distance is 1 mm (the thickness of the PVC tank wall).

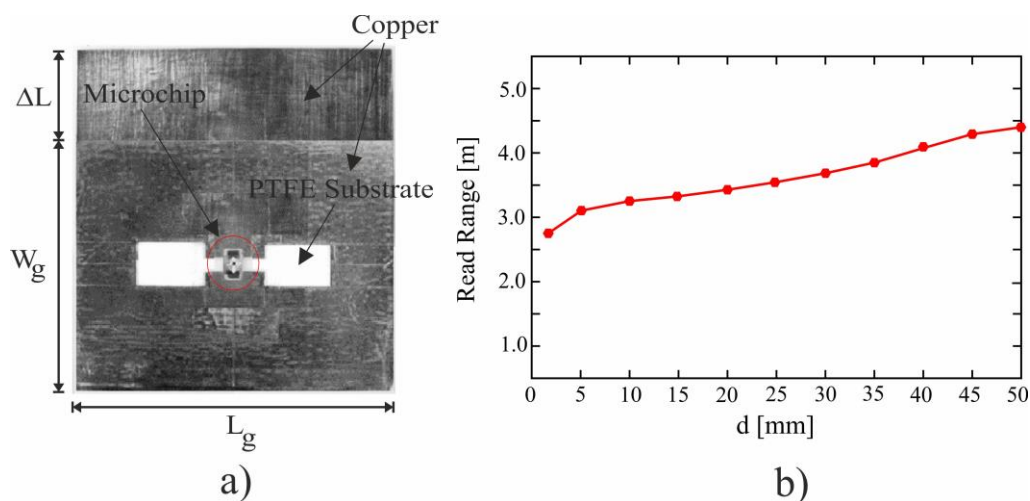


Figure 17. (a) Prototype of the antenna in Figure 3d, with $\Delta L = 30$ mm, $W_g = 49$ mm, $L_g = 60$ mm. (b) Measured read range of the antenna under test.

As in reference [10], the commercial UHF reader Zebra RFD8500 Handheld, fixed on a mobile mount, and remote-controlled by a smartphone application via Bluetooth® wireless technology, is used to measure the read range for the antenna under test.

The spacing between the antenna and the phantom has been modified by using pads of different thickness of expanded polystyrene (EPS), with dielectric permittivity close to 1, and the read range is measured for different spacings between the antenna and the body phantom.

The results of the experimental verification are reported in Figure 17b, and confirm both the robustness of the proposed antenna with respect to its distance by the human-body, as well as the behavior observed in Figure 6 for $\Delta L = 30$ mm. In fact, the read range is very satisfactory for the antenna adherent to the body phantom (which is close to 3 m), and increases when the distance between the antenna and the human body increases. Moreover, the curve of the reading range is very similar to the curve of the simulated $\tau \times \eta$, confirming a good agreement between numerical simulations and experimental validation. The read range measurements have been performed several times, and in Table 1 the results of each measure are reported. For each antenna distance d from the body phantom, ten different measurements were performed, and Figure 17b reports the corresponding mean value of the reading range for the considered distance d .

Table 1. Measured read range of the antenna under test for 10 different measure campaigns. For each antenna distance from the body phantom, the mean value (in green) and the standard deviation (in red) are reported.

	d = 1 mm	d = 5 mm	d = 10 mm	d = 15 mm	d = 20 mm	d = 25 mm	d = 30 mm	d = 35 mm	d = 40 mm	d = 45 mm	d = 50 mm
Measure #1	2.75	3.10	3.30	3.40	3.50	3.65	3.80	3.90	4.00	4.30	4.45
Measure #2	2.80	3.05	3.25	3.30	3.50	3.65	3.85	3.90	4.00	4.25	4.45
Measure #3	2.75	3.15	3.25	3.30	3.45	3.70	3.80	3.95	4.10	4.25	4.40
Measure #4	2.70	3.10	3.20	3.40	3.45	3.60	3.75	3.85	4.10	4.30	4.50
Measure #5	2.80	3.05	3.35	3.35	3.50	3.70	3.90	3.85	4.05	4.35	4.50
Measure #6	2.75	3.20	3.25	3.45	3.40	3.65	3.85	3.80	3.95	4.35	4.40
Measure #7	2.85	3.10	3.30	3.40	3.50	3.70	3.80	3.80	4.05	4.30	4.45
Measure #8	2.70	3.05	3.35	3.30	3.45	3.55	3.75	3.90	4.00	4.20	4.40
Measure #9	2.75	3.15	3.30	3.35	3.55	3.60	3.80	3.95	3.95	4.25	4.50
Measure #10	2.70	3.20	3.20	3.45	3.50	3.55	3.85	3.90	4.00	4.30	4.50
Mean Value [m]	2.755	3.115	3.275	3.37	3.48	3.635	3.815	3.88	4.02	4.285	4.455
Standard Dev.	0.0025	0.0034	0.003	0.0034	0.0018	0.0034	0.0022	0.0029	0.0029	0.0022	0.0019

4. Comparison of Antenna Performance for Different Human Body Models

The robustness of PIFA antennas discussed in Section 2 has been numerically investigated using a simplified three-layer model [7] in the simulated environment, whose electrical parameters are reported in Figure 1. On the other hand, the experimental validation, described in Section 3, has been performed using a simplified phantom, consisting of a PVC tank filled up with a tissue-simulating liquid with muscle-like parameters, because this phantom can be easily implemented. It is therefore important to analyse if the choice of the human body phantom can affect the results. This is an important task, since different parts of the human body should be modelled using different layers, with appropriate thickness and electrical parameters, and wearable devices can be positioned close to different parts of the human body during their normal operation, such as chest, arm, head, leg. In this section, the performance of the PIFA antenna described in Section 2.1, and experimentally validated in Section 3, will be numerically compared considering as human phantoms (Figure 18):

- the three-layer model [7] described in Figure 1;
- the one-layer model [10] used for the experimental validation (Figure 18a);
- the simplified reference model of the human torso (a stratified elliptical cylinder) used in [10] (Figure 18b);
- a simplified model of the human arm (Figure 18c).

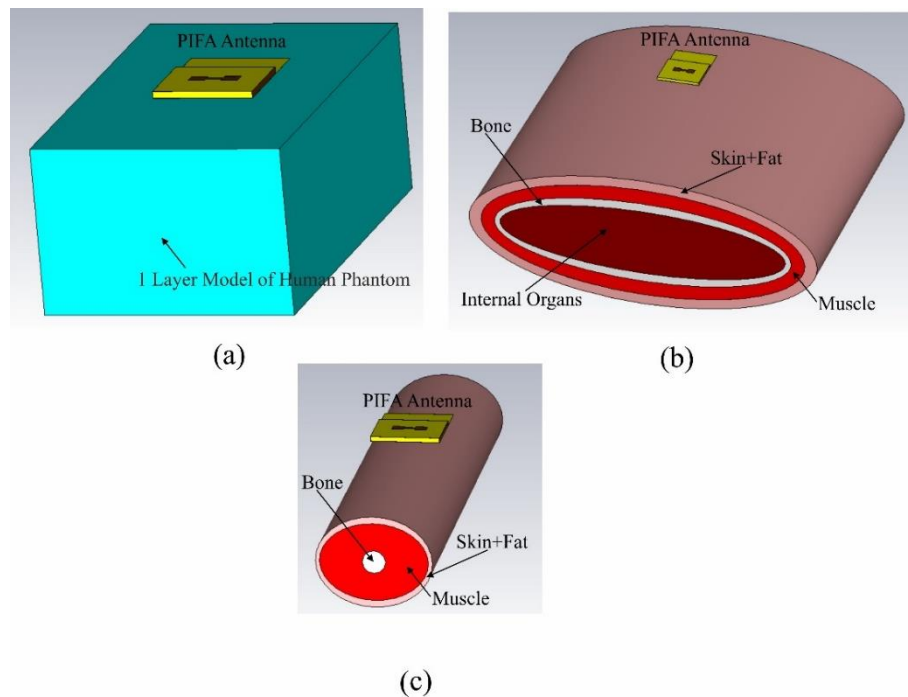


Figure 18. (a) One-layer model (tissue-simulating liquid with muscle-like parameters), with $\epsilon_r = 56.6$ and $\sigma = 1.33$ S/m. (b) Simplified model of the human torso, with parameters: Skin + fat ellipse axes 50×20 cm, $\epsilon_r = 14.5$ and $\sigma = 0.25$ S/m.; Muscle ellipse axes 46.5×17 cm, $\epsilon_r = 55.1$ and $\sigma = 0.93$ S/m.; Bone ellipse axes 42.6×12.6 cm, $\epsilon_r = 20.8$ and $\sigma = 0.33$ S/m.; Internal organs ellipse axes 41×10 cm, $\epsilon_r = 52.1$ and $\sigma = 0.91$ S/m. (c) Simplified model of the human arm, with parameters: Skin + fat ellipse axes 10×8 cm, $\epsilon_r = 14.5$ and $\sigma = 0.25$ S/m.; Muscle ellipse axes 9.5×7.5 cm, $\epsilon_r = 55.1$ and $\sigma = 0.93$ S/m.; Bone ellipse axes 2×2 cm, $\epsilon_r = 20.8$ and $\sigma = 0.33$ S/m.

In Figure 19, the frequency response of the PIFA antenna described in Figure 2, with the optimal extension of the ground plane $\Delta L = 30$ mm, is reported for the four different analyzed human body phantoms for the case of antenna adherent to the human body ($d = 0$ mm). The value of τ is very close for all the considered phantoms, and only a small frequency shift can be observed. This means that the impedance input of the optimized antenna is slightly affected by the human body, even for very different phantom models, and this confirms the high robustness of the optimized antenna. Similar results are obtained in Figure 20, where the variation of τ is reported with respect to the distance from the body phantom for the four different body phantom models considered in the numerical analysis. Figure 21 shows the variation of the efficiency η with respect to the distance from the body phantom, and in this case it is apparent that, while the antenna working in proximity of the three-layer model, the one layer model and the simplified human torso has similar efficiencies, because of the similar extension of these layers, the antenna working close to the human arm model shows a greater efficiency, due to the limited dimension of the arm itself (Figure 18c). Finally, in Figure 22, the variation of $\tau \times \eta$ with respect to the distance from the body phantoms is reported, and the results show a similar behavior of the antenna in presence of very different body phantoms, confirming the very high robustness of the PIFA antenna with optimal ground plane extension ($\Delta L = 30$ mm) with respect to each of the four considered human body models. Therefore, the optimized antenna shows a good robustness regardless of the human body model chosen in the simulation environment.

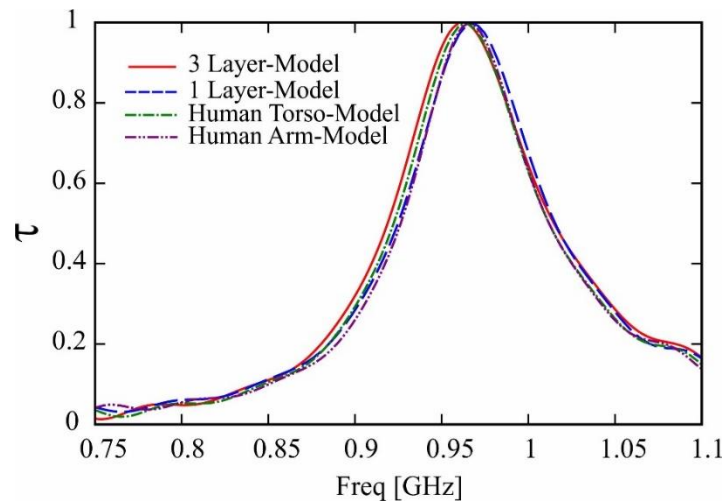


Figure 19. Variation of τ with respect to frequency for different body phantom models.

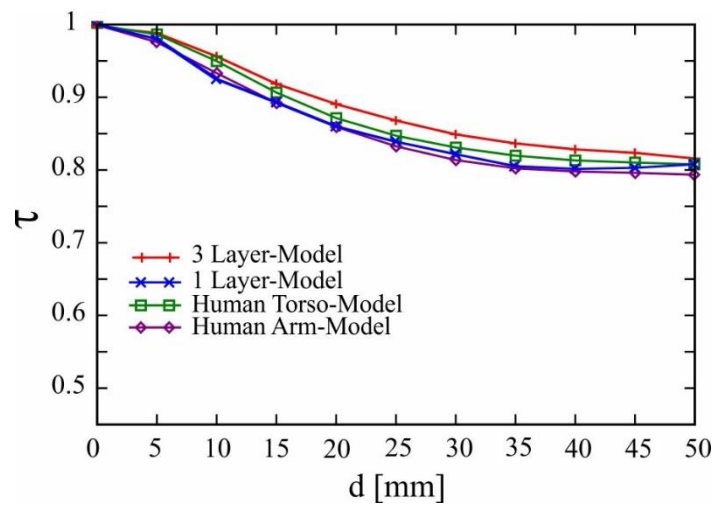


Figure 20. Variation of τ with respect to the distance from the body phantom for different body phantom models.

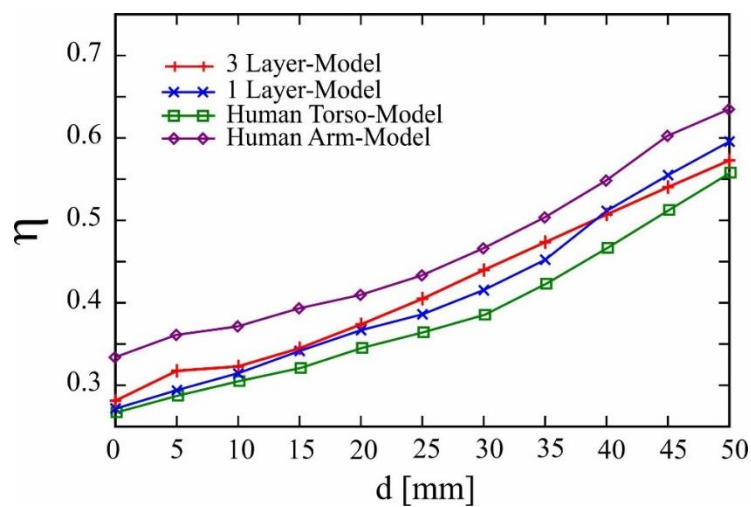


Figure 21. Variation of η with respect to the distance from the body phantom for different body phantom models.

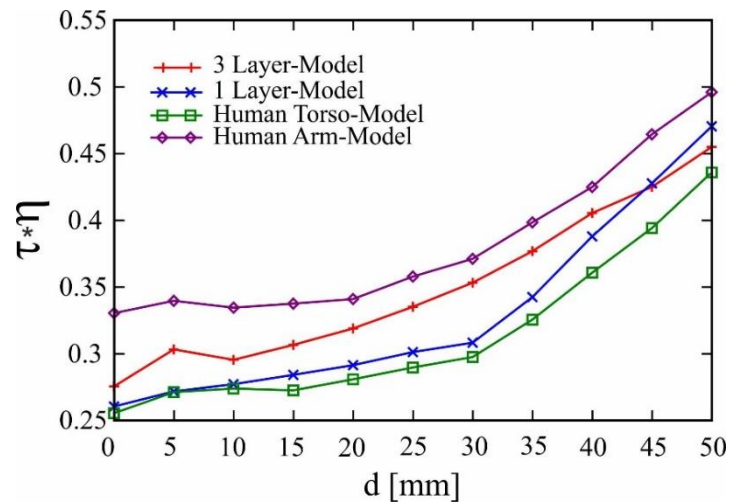


Figure 22. Variation of $\tau \times \eta$ with respect to the distance from the body phantom for different body phantom models.

5. Conclusions

The robustness of the performance of wearable antennas with respect to the human body coupling has been numerically investigated, aiming to an appropriate criterion to choose an optimal extension for the ground plane. The optimal extension of the ground plane has been evaluated both in terms of free space wavelength and in terms of electric energy density magnitude. The best compromise solution found is to extend the ground plane following the profile of the electric energy density. For the presented examples, the optimal extension of the ground plane is equal to $\lambda/10$ and the optimal threshold is equal to $1/1000$ of the maximum value of the electric energy density. The proposed analysis is frequency independent and can be applied to general antenna layouts, allowing us to improve the antenna robustness with respect to the coupling with the human body, but having a minimal impact on the antenna size. The antenna robustness has been compared also using four different models for the human body, showing a similar behavior for all the tested phantoms. The described criterion is therefore very useful for designing wearable pifa antennas, allowing us to easily design compact and robust antennas. Future work will involve the design of new antennas configurations based on the presented rules. Moreover, it should be investigated if this criterion can also be applied when the wearable antenna is bent around the human body (i.e., if the proposed ground plane extension is able to ensure to the wearable antenna an adequate robustness also with respect to flexibility).

Author Contributions: The main contribution to the work has been made by G.A.C., but the contribution of the co-author G.M. has been essential during the review preparation of the article, where substantial modifications and integrations have been made within a very close deadline. Moreover, also in the preliminary phase the suggestions of G.M. helped the author to investigate the problem and to select the most important numerical tests for the structures to investigate. In particular, G.M. contributed to the Investigation, Writing-Review & Editing, and to Funding Acquisition.

Funding: This research received no external funding.

Conflicts of Interest: The author declares no conflict of interest

References

1. Nepa, P.; Rogier, H. Wearable antennas for off-body radio links at VHF and UHF bands (below 1 GHz): Challenges, state-of-the-art and future trends. *IEEE Antennas Propag. Mag.* **2015**, *57*, 30–52. [[CrossRef](#)]
2. PHall, S.; Hao, Y.; Nechayev, V.I.; Alomainy, A.; Constantinou, C.C.; Parini, C.; Kamarudin, M.R.; Salim, T.Z.; Heel, D.T.M.; Dubrovka, R.; et al. Antennas and Propagation for On-Body Communication Systems. *IEEE Antennas Propag. Mag.* **2007**, *49*, 41–58.

3. Islam, M.A.; Kiourti, A.; Volakis, J.L. A Novel Method of Deep Tissue Biomedical Imaging Using a Wearable Sensor. *IEEE Sens. J.* **2016**, *16*, 265–270. [[CrossRef](#)]
4. Merli, F.; Fuchs, B.; Mosig, J.R.; Skrivervik, A.K. The effect of insulating layers on the performance of implanted antennas. *IEEE Trans. Antennas Propag.* **2011**, *59*, 21–31.
5. Casula, G.A.; Altini, M.; Michel, A.; Nepa, P. On the performance of low-profile antennas for wearable UHF-RFID tags. In Proceedings of the 2015 1st URSI Atlantic Radio Science Conference (URSI AT-RASC), Gran Canaria, Spain, 16–24 May 2015.
6. Altini, M.; Casula, G.A.; Mazzarella, G.; Nepa, P. Numerical investigation on the tolerance of wearable UHF-RFID tags to human body coupling. In Proceedings of the IEEE 2015 Antennas and Propagation Symposium, Vancouver, BC, Canada, 20–24 July 2015.
7. Casula, G.A.; Michel, A.; Nepa, P.; Montisci, G.; Mazzarella, G. Robustness of Wearable UHF-Band PIFAs to Human-Body Proximity. *IEEE Trans. Antennas Propag.* **2016**, *64*, 2050–2055. [[CrossRef](#)]
8. Casula, G.A.; Michel, A.; Montisci, G.; Nepa, P.; Valente, G. Energy-Based Considerations for Ungrounded Wearable UHF Antenna Design. *IEEE Sens. J.* **2017**, *17*, 687–694. [[CrossRef](#)]
9. Michel, A.; Colella, R.; Casula, G.A.; Nepa, P.; Catarinucci, L.; Montisci, G.; Mazzarella, G.; Manara, G. Design Considerations on the Placement of a Wearable UHF-RFID PIFA on a Compact Ground Plane. *IEEE Trans. Antennas Propag.* **2018**, *66*, 3142–3147. [[CrossRef](#)]
10. Casula, G.A.; Montisci, G.; Valente, G.; Gatto, G. A robust printed antenna for UHF wearable applications. *IEEE Trans. Antennas Propag.* **2018**, *66*, 4337–4342. [[CrossRef](#)]
11. Casula, G.A.; Montisci, G.; Michel, A.; Nepa, P. Robustness of complementary wearable ungrounded antennas with respect to the human body. *J. Electromagn. Waves Appl.* **2017**, *31*, 1685–1697. [[CrossRef](#)]
12. Casula, G.A. A Design Rule to Reduce the Human Body Effect on Antennas for Short Range NF-UHF RFID Systems. In Proceedings of the 2018 2nd URSI Atlantic Radio Science Meeting (AT-RASC), Meloneras, Spain, 28 May–1 June 2018.
13. Occhiuzzi, C.; Cippitelli, S.; Marrocco, G. Modeling, design and experimentation of wearable RFID sensor tag. *IEEE Trans. Antennas Propag.* **2010**, *58*, 2490–2498. [[CrossRef](#)]
14. Lin, M.-H.; Chiu, C.-W. Human-body effects on the design of card-type UHF RFID tag antennas. In Proceedings of the IEEE International Symposium on Antennas Propag (APURSI'11), Spokane, WA, USA, 3–8 July 2011; pp. 521–524.
15. Lin, C.-H.; Saito, K.; Takahashi, M.; Ito, K. A compact planar inverted-F antenna for 2.45 GHz on-body communications. *IEEE Trans. Antennas Propag.* **2012**, *60*, 4422–4426. [[CrossRef](#)]
16. Hartsgrrove, G.; Kraszewsky, A.; Surowiec, A. Simulated biological materials for electromagnetic radiation absorption studies. *Bioelectromagnetics* **1987**, *8*, 29–36. [[CrossRef](#)] [[PubMed](#)]



© 2019 by the authors. Licensee MDPI, Basel, Switzerland. This article is an open access article distributed under the terms and conditions of the Creative Commons Attribution (CC BY) license (<http://creativecommons.org/licenses/by/4.0/>).